Thermodynamic, Structural and Transport Properties of Tetramethyl Ammonium Fluoride: First Principles Molecular Dynamics Simulations of an Unusual Ionic Liquid

2 AUTHORS, INCLUDING:

Bhabani S. Mallik

Indian Institute of Technology Hyderabad

23 PUBLICATIONS   **203** CITATIONS

Thermodynamic, Structural and Transport Properties of Tetramethyl Ammonium Fluoride: First Principles Molecular Dynamics Simulations of an Unusual Ionic Liquid

Bhabani S. Mallik and J. Ilja Siepmann*

Department of Chemistry and Department of Chemical Engineering and Materials Science, University of Minnesota, 207 Pleasant Street SE, Minneapolis, Minnesota 55455

Received: May 10, 2010; Revised Manuscript Received: August 22, 2010

First principle molecular dynamics (FPMD) simulations in the isobaric−isothermal ensemble were carried out to investigate the liquid phase of pure tetramethyl ammonium fluoride (TMAF), its equimolar mixture with water, and its dilute solution in water. These simulations were performed using Born−Oppenheimer molecular dynamics with the quantum many-body potentials and forces obtained directly from on-the-fly electronic structure calculations at the Kohn−Sham density functional theory level. For the equimolar mixture, simulations were carried out using two different generalized gradient approximation functionals and two values of the charge density cutoff, and it is found that thermodynamic properties are rather sensitive to these details of the electronic structure calculations. The FPMD simulation for neat TMAF at a temperature of 600 K did not yield any indication for the decomposition of TMAF over the 50 ps production period, but trimethylamine and fluoromethane decomposition products were found during a short trajectory at 1200 K. At 400 K and 1 atm, the simulations indicate that significant structural rearrangement and changes in cohesive energy density and compressibility occur upon addition of water to TMAF. The hydration water is found to preferentially solvate the fluoride ions, and the distribution of F^-−H_2O hydrogen bond lifetimes is broad. The simulations do not reveal any significant differences in the transport behavior of TMA^+, F^-, and H_2O over the production periods.

1. Introduction

Ionic liquids (ILs) are an important new class of solvents that have received significant interest due to their technological potential as replacements for traditional organic solvents and due to their unique solubility characteristics.[1−3] The ability to tune their physical and chemical properties through the selection of suitable cations and anions gives ILs a tremendous range of applications, including green chemistry, synthetic chemistry, (bio-) catalysis, and electrochemistry.[1,4−6] In many applications, mixtures of ILs with molecular liquids are used where the latter can induce significant changes in various properties as compared with pure ILs. Due to their hygroscopicity, many ionic liquids can adsorb a significant amount of water from the atmosphere, and in some cases, residual water remains from the synthesis of the ionic liquid.[7,8]

In an effort to decrease the melting point, most common room-temperature ILs contain relatively complex (i.e., bulky and often asymmetric) molecular cations and anions. For special applications, however, less complex constituents can offer advantages. For example, ionic liquids containing the chloride anion possess remarkably solubilizing power for cellulose, presumably because this anion is a strong H-bond acceptor.[9]

The smaller fluoride anion is an even better H-bond acceptor (but less environmentally benign alternative[10]), and Maiti et al.[11] recently proposed ILs with this anion as powerful solvents for materials with a high degree of inter- and intramolecular H-bonding, including 1,3,5-triamino-2,4,6-trinitrobenzene (TATB) and cellulose. In addition, it was suggested by Maiti et al. that cations with smaller alkyl ligands and compact cationic cores,

such as tetramethyl ammonium (TMA), should be better solvents for TATB than the more common alkyl imidazolium ILs.[11]

Beyond its potential as good solvent for TATB, tetramethylammonium fluoride (TMAF) has also been used in synthetic applications both as a reagent and as a catalyst.[12−15] In the solid state, TMAF can exist in an anhydrous form[13] and in four crystalline hydrates.[16] Melting temperatures are not known for the anhydrous form and the monohydrate of TMAF (but the higher hydrates melt at temperatures between 283 and 319 K[16]); in dynamic vacuum, the anhydrous form starts to decompose into trimethylamine and fluoromethane at temperatures above 440 K.[13] Furthermore, the high solubility of TATB in fluoride-containing ILs may involve the formation of a Meisenheimer complex, that is, a σ bond between the F^- anion and an amine carbon of TATB, or a hydrogen abstraction from one of the amine groups.[11] Thus, TMAF is a somewhat unusual ionic liquid because of its small and highly symmetric cation, very small, and highly reactive anion and its use as reagent and catalyst.

To our knowledge, the liquid phase of anhydrous or hydrous TMAF has not yet been investigated by experimental or computational means. Over the past decade, molecular simulation studies have greatly aided in predicting and understanding the properties of ILs, and first principles, molecular mechanics (atomistic), and coarse-grain descriptions have been employed in these studies (for excellent reviews, see refs 17−22). Simulations have also been used extensively to investigate the properties of mixtures of ILs and water.[17,23−26]

In this work, first principles molecular dynamics (FPMD) simulations were used to probe the liquid phases of anhydrous and hydrous TMAF (using an equimolar mixture of water and TMAF corresponding to the monohydrate) and its dilute aqueous solution. A first principles representation was used here because of the potential for TMAF to decompose at elevated tempera-

---

TABLE 1: Simulation Details (System, Electronic Structure Parameters, Temperature, and Length of Production Period) and Thermodynamic Properties (Specific Density, Isothermal Compressibility, Cohesive Energy, and Cohesive Energy Density)[a]

system TMAF	model	T (K)	t (ps)	ρ (kg/m^3)	κ_T (10^{-11} Pa^{-1})	ΔU_{coh} (kJ/mol)	ρ_U (J/cm^3)	ΔU_{DZVP}^{20} (kJ/mol)	ΔU_{TZV2P}^{20} (kJ/mol)
anhydrous	BLYP-300	400	32	830 ± 20	43 ± 1	80 ± 1	720 ± 20	77	63
anhydrous	BLYP-300	600	48	650 ± 20	93 ± 3	67 ± 1	470 ± 20	66	53
hydrous	BLYP-300	400	36.3	720 ± 20	66 ± 2	66 ± 2	880 ± 20	67	61
hydrous	BLYP-600	400	25.9	640 ± 20	73 ± 3	71 ± 2	800 ± 30	72	62
hydrous	PBE-300	400	22.6	740 ± 20	51 ± 2	67 ± 2	880 ± 20	65	54
solution	BLYP-300	400	25	760 ± 20	51 ± 2				

[a] The last two columns give averages computed from only 20 configurations.

tures[13] (which may lead to the inadvertent production of hydrofluoric acid[10]) and because subsequent work will investigate the solvation of TATB in TMAF, a process that may involve reactive events. All first principles simulations were carried out in the isobaric−isothermal ensemble to allow the systems to find their equilibrium densities, and the sensitivity of the predictions to the density functional and the plane wave cutoff was also explored for hydrous TMAF. This paper is organized as follows: technical details of the FPMD simulations are described in section 2; the thermodynamic, structural, and transport properties of the various TMAF systems are discussed in section 3; and concluding remarks follow.

2. Computational Methods

FPMD simulations were carried out using the efficient Quickstep routines[27] of the CP2K simulation package (http://cp2k.berlios.de). Energies and forces were calculated using the Gaussian plane wave method,[27,28] which employs a dual basis set formalism of Gaussian-type orbitals and plane waves for the electronic density to solve the self-consistent Kohn−Sham equations of density functional theory.[29] In the simulations using CP2K, the system is always kept in the electronic ground state corresponding to Born−Oppenheimer molecular dynamics.

The majority of the FPMD simulations used the Becke−Lee−Yang−Parr (BLYP) exchange/correlation functionals[30,31] with the norm-conserving Goedecker−Teter−Hutter pseudopotentials for the core electrons,[32,33] a double-ζ valence plus polarization (DZVP) basis set, and a plane wave cutoff at 300 Ry (this set of electronic structure parameters is abbreviated here as BLYP-300). For hydrous TMAF, additional simulations were performed using the Perdew−Burke−Ernzerhof exchange/correlation functionals[34] (called here PBE-300) and a larger plane wave cutoff of 600 Ry for the BLYP functional (BLYP-600).

The FPMD simulations were carried out in the isobaric−isothermal ensemble where massive Nose−Hoover chain thermostats[35] were used to control the temperature, and the pressure was controlled via the barostat suggested by Mundy and co-workers.[36] An external pressure of 1 atm was applied to all simulations, and the temperature was set to 400 K for most of them. The integration time step was set to 0.5 fs.

Systems with three different compositions were explored: (i) anhydrous TMAF consisting of 16 ion pairs, (ii) an equimolar mixture of TMAF and water consisting of 16 ion pairs and 16 water molecules, and (iii) a dilute aqueous solution of TMAF consisting of one ion pair and 50 water molecules. The systems were pre-equilibrated using Monte Carlo simulations in the isobaric−isothermal ensemble with TMAF interaction parameters derived from the TraPPE force field[37] and the SPC/E model for water,[38] followed by a geometry optimization in CP2K before starting the FPMD simulations. An equilibration period of 10 ps that was found to be sufficiently long for the cell volume

and system energy to stabilize was used for all systems. This was followed by production periods ranging from 22 to 48 ps. All properties were averaged over the production period, and the uncertainties (standard deviations) were estimated by dividing this period into five blocks. The exception was one simulation for anhydrous TMAF at a temperature of 1200 K that was started from the final configuration at 600 K and run only until the first two decomposition events occurred (i.e., the results reported for the 1200 K simulation do *not* include an equilibration period and indicate the response of the system immediately following the instantaneous jump in the temperature from 600 to 1200 K). Information on the simulation parameters, temperature, and length of all simulations is summarized in Table 1.

The configurations at every time step were written to a file for subsequent analysis. The radial distribution functions (RDFs) were computed using a bin width of 0.02 Å for $r < 4.0$ Å and a larger bin width of 0.1 Å for the remainder.

3. Results and Discussion

3.1. Thermodynamic Properties. The ensemble-averaged values for the specific density, isothermal compressibility, cohesive energy, and cohesive energy density are listed in Table 1. For anhydrous TMAF, a liquid density of 830 kg/m^3 is found at 400 K, and it decreases to 650 kg/m^3 when the temperature is raised to 600 K. As noted above, experimental information is not available for the liquid phase, but a specific density of 1058 kg/m^3 has been calculated from the powder pattern of the solid form at ambient conditions.[13] Determining the coefficient of thermal expansion from the two simulations, one can extrapolate a specific density of about 920 kg/m^3 for the (metastable) liquid at 300 K, a value that is not unreasonable, considering a likely density difference between solid and liquid forms of anhydrous TMAF and the fact that the BLYP functional (with a similar charge density cutoff) has been shown to underpredict the density of liquid water by about 10−15%.[39]

For hydrous TMAF, we obtain specific densities of 720, 640, and 740 kg/m^3 for simulations with BLYP-300, BLYP-600, and PBE-300, respectively. As also found for liquid water,[39,40] the specific density (and also other thermodynamic properties) are quite sensitive to the exchange/correlation functional and the charge density cutoff. In agreement with previous simulations for liquid water, increasing the charge density cutoff appears to lead to a decrease in the density (a cutoff at 1200 Ry was found sufficient to yield nearly converged energy−volume curves for liquid water, but such a high cutoff would be too expensive for the larger systems studied here),[39] and the PBE representation yields a higher density than BLYP representation.[36,40] As one might expect, the density of the hydrous form is somewhat lower (by ∼15%) than that for the anhydrous form for the same electronic structure parameters (i.e., BLYP-300). The density of 760 kg/m^3 found for the dilute solution of TMAF

Properties of TMAF

J. Phys. Chem. B, Vol. 114, No. 39, 2010 **12579**

is consistent with previous FPMD simulations for neat water[41] when accounting for the difference in charge density cutoff and basis set. A comparison of the specific densities for the anhydrous and hydrous forms and for the dilute solution indicates a positive excess volume of mixing.

The isothermal compressibility of these systems can be estimated directly from the volume fluctuations encountered during the simulations in the isobaric–isothermal ensemble; the corresponding values are listed in Table 1. All compressibilities are of the same magnitude (ranging from 4 to 9×10^{-10} Pa^{-1}) and fall in the range observed for other ionic liquids and water.[42,43] The κ_T value is smaller for the anhydrous form than for the hydrous form, presumably due to a reduction (i.e., shielding) in the Coulombic interactions. Comparing the different functionals/cutoffs, we find that those yielding a higher density give a smaller compressibility.

The cohesive energy, ΔU_{coh}, is a measure of the strength of the intermolecular interactions in a condensed phase relative to isolated molecules. Here, ΔU_{coh} for the IL phases is given in terms of formula units (e.g., TMAF· H$_2$O is considered as two units) and computed as follows. The energy of a single TMAF ion pair and separately of an isolated water molecule (only for hydrous TMAF) is computed from brief simulations in the canonical ensemble using the average volume obtained from the simulations of the corresponding liquid phase. The difference in this energy for the isolated species and the liquid phase is taken as ΔU_{coh} and reported in Table 1. At the same temperature (400 K) and for the same electronic structure parameters (BLYP-300), ΔU_{coh} for the anhydrous form is nearly 20% larger than for the equimolar mixture of TMAF and water; that is, the addition of water appears to weaken the interactions between the constituents. This result is consistent with the lower melting temperature of the higher hydrates.[16] However, due to the relatively small partial molar volume of the hydration water, the cohesive energy density is actually higher for the hydrous form than for the anhydrous form of TMAF.

Out of necessity, a relatively small basis set had to be used for the simulations of these large systems. To assess the effect of the basis set size, the energy was recalculated at the DZVP and TZV2P levels for 20 configurations equally spaced in time from the production periods for each liquid phase and corresponding vapor-phase cluster. As can be seen from the data listed in Table 1, the average cohesive energies for these 20 configurations at the DZVP level agree well with the ensemble averages over the entire production periods. In contrast, the average cohesive energies for these 20 configurations at the TZV2P are ~20% smaller in magnitude; that is, the simulations at the DZVP level overestimate the cohesive energy. This finding is in agreement with previous first principles simulations that found a larger heat of vaporization at the DZVP than TZV2P level for water.[40]

3.2. Structure and Stability. A. *Structure and Stability of Anhydrous TMAF.* The atom–atom RDFs and the corresponding number integrals (NIs) for anhydrous TMAF at 400 and 600 K are shown in Figure 1. Let us discuss first the structure at the lower temperature. For the N–N and F–F RDFs, the maxima for the first peak are found at 6.2 and 6.3 Å, respectively, and the first minima fall just outside half of the linear dimension of the simulation boxes. Nevertheless, the N–N and F–F NIs indicate coordination numbers of 11 and 10, respectively. The N–C and C–C RDFs exhibit the characteristically sharp peaks for bonded interactions at 1.53 and 2.49 Å with the expected coordination numbers of 4 and 3, respectively. The first intermolecular feature is a shoulder in
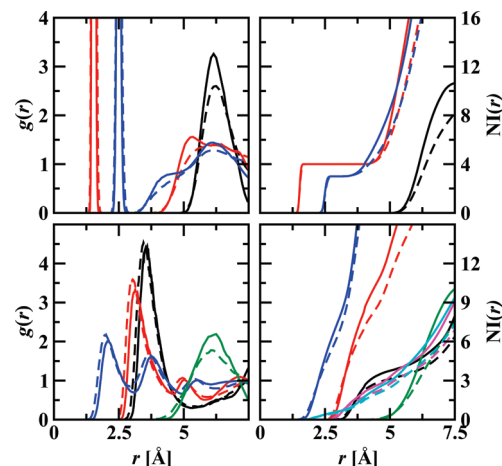

Figure 1. Radial distribution functions (left) and corresponding number integrals (right) for anhydrous TMAF. The top part depicts the cation structure with the black, red, and blue lines indicating N–N, N–C, and C–C pairs, respectively. The bottom part depicts the pairs involving the anion with the black, red, blue, and green lines indicating F–N, F–C, F–H, and F–F pairs, respectively. For the mixed pairs, the magenta and cyan lines show C–F and H–F number integrals, respectively. The solid and dashed lines show the results at 400 and 600 K, respectively. Note that the average linear dimensions of the simulation boxes are 14.4 and 15.6 Å, respectively.

the C–C RDF at 4.3 Å; that is, a little larger separation than observed for branched alkanes.[44] The corresponding NI reaches a value of 7 at $r \approx 4.8$ Å and, hence, indicates that the orientations of neighboring cations are only weakly correlated (NI values of 4 or 6 would have indicated that a methyl group points toward another or between three other methyl groups, respectively). Similarly, the second (i.e., first intermolecular) peak in the N–C RDF at 5.3 Å is relatively weak, and there are no significant minima separating the third and fourth peak.

The RDFs involving anion–cation sites exhibit significantly more structuring. The F–N RDF shows a strong peak at 3.6 Å and a pronounced minimum at 5.3 Å with the corresponding coordination number being close to 4; that is, each anion is surrounded by 4 cations and vice versa. From the powder pattern of anhydrous TMAF, a hexagonal unit cell with an *anti*-NiAs-type structure was deduced in which the anion–cation and cation–anion coordination numbers are six,[13] that is, there is less coordination in the liquid phase.

The first peak in the F–C RDF is located at 3.1 Å and shows significant asymmetry. The first minimum is found at 4.6 Å and is followed by a small second peak at 5.0 Å before a deeper minimum is reached at 5.8 Å. The coordination numbers up to these minima are 11 and 17, respectively; that is, it appears that the four cations are preferentially oriented with three methyl groups pointing toward the closest anion. The coordination number from the C–F NI at 4.6 Å is close to 3. As should be expected, the F–H RDF exhibits the intermolecular peak with the shortest separation at 2.1 Å, that is, significantly longer than the H-bonded peak in molecular hydrogen fluoride.[45] Its first minimum is found at 3.1 Å, and the F–H and H–F coordination numbers are 8 and 0.7, respectively.

The increase in temperature from 400 to 600 K leads only to subtle changes in the RDFs, and there is no indication for the formation of decomposition products (trimethylamine and fluoromethane; that is, each N atom remains surrounded by exactly four carbon atoms within $r < 1.9$ Å, and no F atoms are found closer than 2.2 Å to a C atom) nor for the formation of hydrofluoric acid. Of course, the nonbonded NIs show signifi-
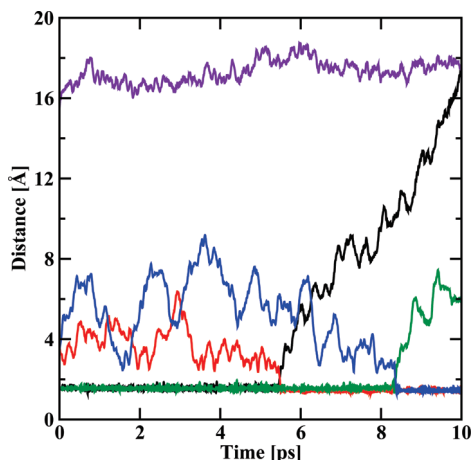
Figure 2. Trajectories of the N−C and F−C distances involved in two reactive events at 5.5 and 8.4 ps. The N−C distances are depicted by the black and green lines; the corresponding F−C distances, by the red and blue lines; and the box length, by the purple line. Periodic boundary conditions were not applied in the computation of the separation distances.

Figure 3. Snapshots illustrating the first decomposition event: (A) The TMA$^+$ and F$^-$ ions at $t = 4$ ps. (B) The trimethylamine and fluoromethane decomposition products at $t = 7$ ps. (C) The reactive complex at the time when the N−C and F−C distances are equal ($t = 5.48$ ps, $d = 2.07$ Å). Orange, green, gray, and purple indicate N, C, H, and F, respectively.

cant downward shifts due to the decrease in density. Nevertheless, the first peak positions for the N−N and F−F RDFs are not found to be shifted to larger distances, but their heights are decreased at the higher temperature. To the contrary, the first peaks of the F−N, F−C, and F−H RDFs are all shifted to smaller separations by about 0.1 Å and are somewhat larger in height at 600 K. Presumably, these changes are caused by incomplete coordination shells for these anion−cation interactions that lead to closer separations for the remaining neighbors. The N−C and C−C RDFs show the most significant changes upon the temperature increase. The triple peak in the N−C RDF ($5.3 < r < 7.0$ Å) has merged into one broad peak, and the shoulder at 4.3 Å in the C−C RDF is much less pronounced.

Experimental studies[12,13] have found that anhydrous TMAF decomposes at elevated temperatures. Christe et al.[13] investigated the decomposition of TMAF and observed that it starts to slowly decompose at temperatures above 440 K in a dynamic vacuum and quantitatively pyrolyzes at 480−500 K, with trimethylamine and fluoromethane as the decomposition products. Clearly, the higher simulation temperature of 600 K falls well above the experimentally reported decomposition temperature, but no decomposition was observed over more than 50 ps (including the equilibration period). This is not unexpected because even the decomposition of a single TMAF ion pair would constitute an exceedingly fast decomposition rate of 10^9 mole s^{-1}.

Thus, a simulation at 1200 K was initialized from the final configuration at 600 K (i.e., the kinetic temperature was instantaneously doubled and thereafter maintained through the massive thermostats). During this 1200 K simulation, the atom−atom distances were monitored for any breakage of a N−C bond and formation of a F−C bond (or F−H bond), and two decomposition events were observed. The trajectories of the relevant atom−atom distances and of the box length are depicted in Figure 2.

The first reactive event occurs at 5.5 ps and is followed by a second event at 8.4 ps. In both cases, a F$^-$ anion first approaches a C atom relatively closely, and their separation fluctuates around 2.6 Å before a sudden concomitant lengthening of the N−C bond and shortening of the C−F bond occurs. In both cases, the trajectories cross at a separation of about 2.05 Å and the C−F bond is rapidly formed. These reactive events take place within about two vibrational periods for the N−C and
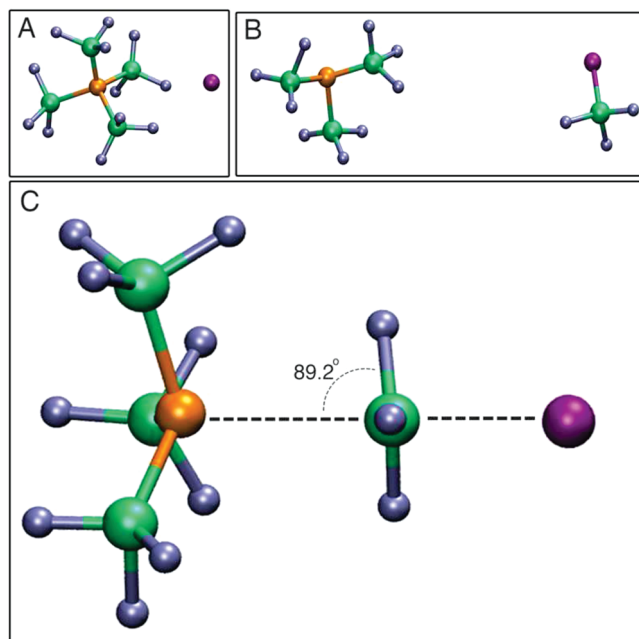
C−F bonds. Snapshots illustrating the first reactive event are shown in Figure 3. It appears that the reaction proceeds through an umbrella inversion, and at the point when the N−C and C−F distances are equal, all H−C−X (with X being N or F) angles are very close to 90°, and the N−C−F angle is close to 180°. It is encouraging that the 1200 K simulation yields the same decomposition products as found in the experimental pyrolysis.[13] It should also be noticed that the box length increases only slowly over the 10 ps trajectory at 1200 K; that is, anhydrous TMAF decomposes in the condensed phase but one may expect a phase change to occur after additional decomposition events at this extremely high temperature.

B. Structure of Hydrous TMAF and its Dilute Aqueous Solution. TMAF is very hygroscopic due to the high charge density of the fluoride anion, and one should expect that addition of water may lead to significant structural rearrangements compared to the anhydrous form. Furthermore, different combinations of functional/charge density cutoff were used for the TMAF monohydrate, and the large differences observed in the thermodynamic properties may also be reflected in structural differences.

Let us discuss first the ion−ion structure (see Figure 4). Compared with the anhydrous form, the position of the first peak in the N−N RDF is shifted outward by ∼0.1−6.3 Å, but more importantly, the peak height is decreased by ∼25%, and the first minimum is significantly less pronounced for the hydrous TMAF. The value of the N−N NI at 7.5 Å is only about 7 for the hydrous TMAF. Although the differences between the different electronic structure parameters are small for the N−N RDFs, the lower density for BLYP-600 results in a smaller NI at the same separation. The position of the first peak in the F−N RDF does not show a systematic shift between the anhydrous and hydrous forms but for the same electronic structure parameters (BLYP-300), the peak height is significantly reduced for the hydrous form. In contrast, the depth of the first minimum is clearly more pronounced for anhydrous TMAF than
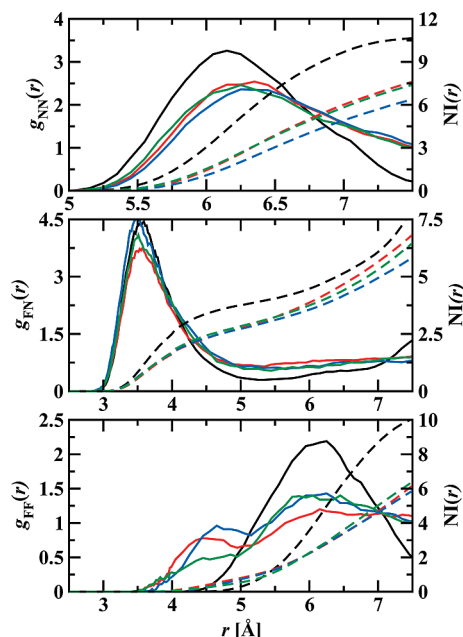
Properties of TMAF

J. Phys. Chem. B, Vol. 114, No. 39, 2010 **12581**

Figure 4. Comparison of the radial distribution functions (—) and number integrals (— — —) for anhydrous and hydrous TMAF at 400 K. The top, middle, and bottom parts show data for N–N, F–N, and F–F pairs, respectively. The black, red, blue, and green lines depict anhydrous TMAF and hydrous TMAF with the BLYP-300, BLYP-600, and PBE-300 descriptions, respectively.

for hydrous TMAF with all three descriptions, whereas the coordination number at 5.3 Å decreases from 4 for anhydrous TMAF to 3 for hydrous TMAF. Possibly the most interesting change in ion–ion structure is observed for the F–F RDF, in which a shoulder at shorter separations ($r \approx 4.5$ Å) emerges for hydrous TMAF, and concomitantly, the height of the peak at $r \approx 6$ Å is greatly reduced compared with anhydrous TMAF. The shoulder is a signal for water-separated anion pairs (see below).

Additional insight can be gained from cation–water and anion–water RDFs and NIs for hydrous TMAF and the dilute aqueous solution of TMAF. Figure 5 shows the RDFs and NIs for N–O and C–O pairs. In both cases, the general features for the RDFs for hydrous TMAF with the three different electronic structure parameters are quite similar, whereas the RDFs for the aqueous solution differ markedly. The N–O RDF for hydrous TMAF shows a broad first peak at $r \approx 4.4$ Å and a deep minimum at $r \approx 6.8$ Å, where the NIs reach a value of ~ 5.

In contrast, the aqueous solution shows a double peak ($r \approx 4.8$ and 5.9 Å) with low height, and there is no clear minimum in the RDF until half the box length is reached. For the C–O RDF, the hydrous TMAF systems exhibit a first peak at $r \approx 3.7$ Å, followed by a much smaller secondary peak at $r \approx 5.4$ Å, and the corresponding coordination numbers are 1.8 and 5.5 (with slightly smaller values for the less-dense PBE-300 system). Thus, it appears that two water molecules are in close proximity of each methyl group. Again, the structure around the cation is much less well-defined for the aqueous solution, with the first feature being a shoulder, followed by a broad peak that is shifted outward compared with hydrous TMAF.

Figure 6 depicts the anion–water RDFs and NIs. The first peak of the F–O and F–H RDFs are very significantly enhanced for hydrous TMAF compared with the aqueous solution, that is, an indication for the microheterogeneity of hydrous TMAF where water preferentially solvates the fluoride ion with its
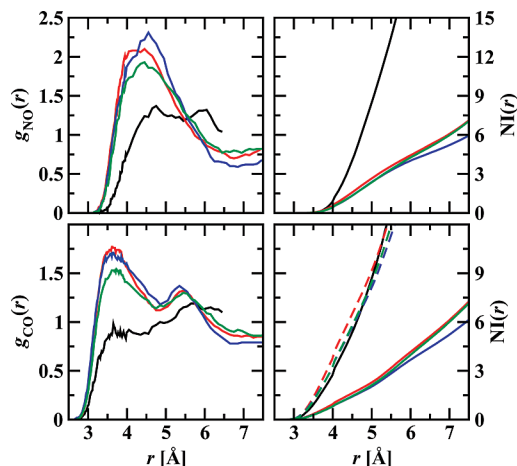

Figure 5. Comparison of the cation–water radial distribution functions and number integrals for hydrous TMAF and the dilute solution. The top and bottom part show data for N–O and C–O, respectively. The black, red, blue, and green lines indicate the data for the dilute solution and hydrous TMAF with the BLYP-300, BLYP-600, and PBE-300 descriptions, respectively. The dashed lines (only for hydrous TMAF) show the corresponding O–C number integrals, respectively. Note that the average linear dimensions of the simulation box for the dilute solution is only 12.9 Å.
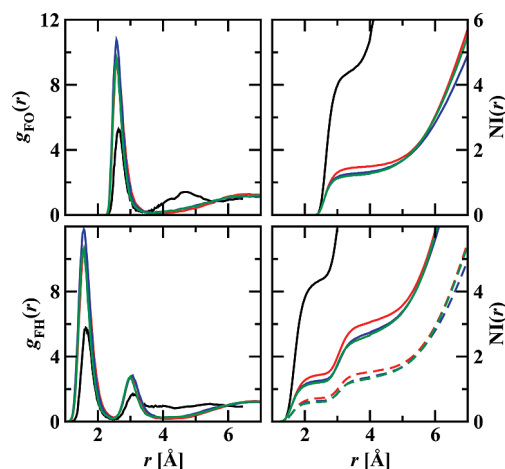

Figure 6. Comparison of the anion–water radial distribution functions and number integrals for hydrous TMAF and the dilute solution. The top and bottom part show data for F–O and F–H, respectively. The black, red, blue, and green lines indicate the data for the dilute solution and hydrous TMAF with the BLYP-300, BLYP-600, and PBE-300 descriptions, respectively. The dashed lines (only for hydrous TMAF) show the corresponding H–F number integrals.

higher charge density. Although the peak heights for the BLYP-300 and PBE-300 descriptions are rather similar, the width is slightly larger for BLYP-300, and correspondingly, the coordination numbers for the first solvation shell are slightly higher, with F–O values of 1.5 and 1.3 and F–H values of 1.4 and 1.2 for BLYP-300 and PBE-300, respectively. The corresponding values for the aqueous solution are 4.4 and 4.3 for F–O and F–H. The F–H RDFs show the characteristic double peak for strongly directional hydrogen bonding, with the first peak at $r \approx 1.6$ Å originating from one hydrogen atom of each water molecule being pointed toward the fluoride ion. The second peak at $r \approx 3.0$ Å (a distance slightly larger than the position of the first peak in the F–O RDFs) is due to the second hydrogen atom of the same water molecule pointing away from the fluoride ion. It should also be noted that the simulations do not yield an indication for the formation of hydrofluoric acid from hydrous TMAF.
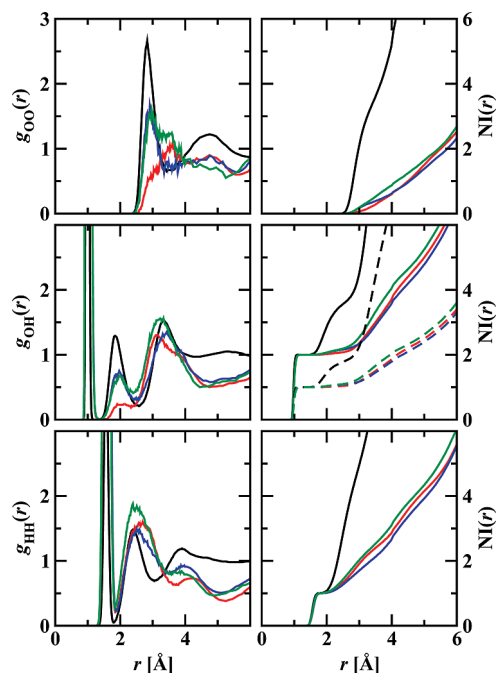
Figure 7. Comparison of the water–water radial distribution functions and number integrals for hydrous TMAF and the dilute solution. The top, middle, and bottom parts show data for O–O, O–H, and H–H, respectively. The black, red, blue, and green lines indicate the data for the dilute solution and hydrous TMAF with the BLYP-300, BLYP-600, and PBE-300 descriptions, respectively. The dashed lines show the corresponding H–O number integrals.

The F–O RDF for the aqueous solution shows a significant second peak at $r \approx 4.7$ Å, that is, a clear second solvation shell that is absent for hydrous TMAF; that is, water molecules in the first solvation shell of the fluoride ion are not strongly coordinated with secondary water molecules. This is further supported by analysis of the water–water RDFs (see Figure 7). The O–O and O–H RDFs for BLYP-600 and PBE-300 show only weak peaks at the typical H-bonding separations ($r_{OO} \approx 2.8$ Å and $r_{OH} \approx 1.9$ Å for the aqueous solution), and the peak is further diminished to a shoulder for the BLYP-300 simulation. However, it should be noticed that these differences may also be caused by insufficient sampling because the O–O coordination numbers at $r = 3.5$ Å are only 0.2, 0.3, and 0.4 for BLYP-300, BLYP-600, and PBE-300. Nevertheless, it is clear that all simulations for hydrous TMAF yield much stronger structuring for F–O than for O–O.

The relatively large third peak in the O–H RDFs ($r \approx 3.3$ Å) and second peak in the H–H RDFs ($r \approx 2.5$ Å) for hydrous TMAF originate from two water molecules bound to the same fluoride ion. The preference for water molecules to associate more strongly with small anions than with other water molecules has also been observed in simulations of equimolar 1,3-dimethylimidazolium chloride/water mixtures.[26] Comparing the water–water RDFs for the hydrous form with those obtained for the dilute solution, we observe that the first intermolecular O–O and O–H peaks are significantly more pronounced for the dilute solution; that is, the water–water interactions are relatively weak for the hydrous form.

3.3. Hydrogen Bond Properties. As indicated by the RDFs, the water molecules in hydrous TMAF associate more strongly with the fluoride ions than with themselves. Each water molecule can form up to four hydrogen bonds (two as a donor and two as an acceptor) but the fluoride ion can act only as an H-bond acceptor. Thus, fluoride ions can be characterized according to

TABLE 2: Percentages of Fluoride Ions and Water Molecules in Specific H-Bonded Arrangements in Hydrous TMAF[a]

Model	Species	0A	1A	2A	3A
BLYP-300	F⁻	18	34	28	18
BLYP-600	F⁻	16	46	29	8
PBE-300	F⁻	25	30	32	8

Model	Species	0F0D0A	1F0D0A	2F0D0A	1F1D0A	1F0D1A
BLYP-300	H_2O	8	35	29	8	5
BLYP-600	H_2O	5	44	28	5	6
PBE-300	H_2O	8	29	33	8	6

[a] Only species with populations of 5% and above are listed.

the number, a, of H-bonds accepted as aA species. Similar, the water molecules can be placed into groups with the descriptor fFdDaA, where f, d, and a are the numbers of H-bonds donated to a fluoride ion, donated to another water molecule, and accepted from another water molecule, respectively. To carry out this analysis, one needs to define the criteria for F⁻–H_2O and H_2O–H_2O H-bonds. In this work, we used a combined distance-angular criterion; that is, a F⁻–H_2O H-bond is present when the following conditions are met: $r_{FO} \leq 3.4$ Å, $r_{FH} \leq 2.6$ Å, and $\cos \theta_{OH-F} \leq -0.1$, where r_{FO}, r_{FH}, and $\cos \theta_{OH-F}$ are the ion–oxygen distance, the ion–hydrogen distance, and the angle between the O–H bond vector and the F⁻–H H-bond vector. For two water molecules, an analogous set of conditions must be met: $r_{OO} \leq 3.3$ Å, $r_{OH} \leq 2.5$ Å, and $\cos \theta_{OH-O} \leq -0.1$.[46] Any H-bond criterion has a certain level of arbitrariness, and any change in the criterion will lead to changes in the population of a particular species. Nevertheless, the same trends emerge with any reasonable H-bond criterion, and the physical insight is not altered by changing between these criteria.[47,48] It should be noted here that the combined distance–angular criterion does not allow for a water molecule to form two hydrogen bonds with the same F⁻ acceptor, but the close agreement of the first plateau values for the F–O and F–H NIs (see Figure 6) indicates that water molecules prefer an orientation with only one H atom pointing toward the fluoride ion.

Numerical values for the H-bond speciation of the fluoride ion and the water molecules are reported in Table 2. For all three electronic structure descriptions, it is found that the 1A and 2A species are most prevalent for the fluoride ion, and these two groups together make up about two-thirds of the fluoride ions. Around one-fifth of the fluoride ions is found without a H-bonded water molecule (species 0A) and 10–20% are H-bonded to 3 or more water molecules. This species distribution leads to an average of 1.3–1.5 H-bonds per fluoride ion. Since the number of fluoride ions and water molecules is equal in the hydrous TMAF systems, some of the water molecules must form a bridge between two fluoride ions (as already indicated by the O–F coordination numbers being larger than unity). Indeed, about one-third of the water molecules have speciation 2F0D0A, that is, form H-bonds to two fluoride ions but not any water molecules. These water bridges explain the shoulder in the F–F RDF at $r \approx 4.5$ Å (see Figure 4). Bridging water molecules have also been found in simulations of 1,3-dimethylimidazolium chloride/water mixtures.[26,49] The other water species with a population of about one-third in hydrous TMAF is 1F0D0A, that is, again forming an H-bond only with the fluoride ion. Only about a quarter of the water molecules are involved in a hydrogen bond with another water molecule, and of those, the 1F1D0A and 1F0D1A species are most
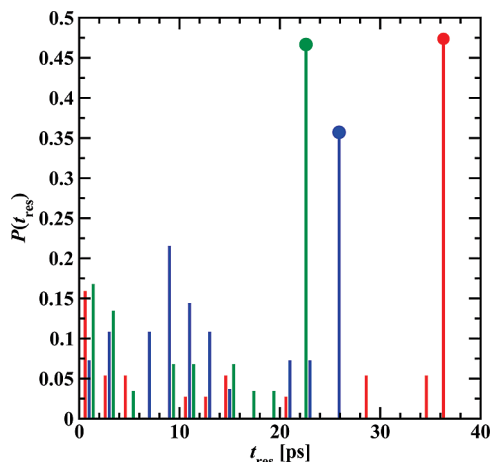
Properties of TMAF

J. Phys. Chem. B, Vol. 114, No. 39, 2010 **12583**

Figure 8. Probability distributions for the H-bond lifetime of a water molecule bonded to a specific fluoride ion for hydrous TMAF. The red, blue, and green bars depict data obtained for the BLYP-300, BLYP-600, and PBE-300 descriptions, respectively. The analysis considers only the production period for each system, the bin width is 2 ps, and the bars with the filled circle indicate the end of each production period.

Figure 9. Mean square displacements of TMA^+, F^-, and H_2O in anhydrous and hydrous TMAF. Solid black, dashed black, red, blue, and green lines depict the data for anhydrous TMAF at 400 and 600 K, and hydrous TMAF with the BLYP-300, BLYP-600, and PBE-300 descriptions, respectively. In the logarithmic plots, the black dotted line indicates a slope of 1. In the linear plots, the black dotted lines indicate diffusion coefficients of 0.2 and 2.0×10^{-5} cm^2 s^{-1}.

prevalent. The number of water molecules not involved in any H-bond is rather small.

The distribution of H-bond lifetimes that a water molecule remains H-bonded to the same fluoride ion is depicted in Figure 8. Using the relatively strict H-bond criterion of this work, water molecules sometimes "escape" for a short time interval before connecting again with the same fluoride ion. To account for this, a H-bond is considered as broken only when a reconnection is not made within 2 ps. Unfortunately, the FPMD simulations are too short to yield smooth distributions because, on average, a F^-–H_2O hydrogen bond is broken in these systems only about once per picosecond. Nevertheless, the distributions for the three electronic structure descriptions are sufficiently similar that some qualitative observations can be made: ∼20−40% of the residence times are relatively short-lived ($t_{res} < 6$ ps), ∼20−40% exhibit intermediate residence times ($6 < t_{res} < 16$), and nearly half of the H-bonds remain stable over the entire production period (with this fraction being somewhat lower for the BLYP-600 run with its lower density). Given the insufficient number of H-bond formation/breakage events, no attempt is made here to group the residence times to the different H-bonded species discussed above.

3.4. Transport Properties. It is natural to use a molecular dynamics trajectory also to compute transport properties. However, given the relatively short run times that are accessible to FPMD simulations[50] and the long relaxation times that ionic liquids are known for,[19] extreme caution is warranted regarding any quantitative prediction of transport properties. The self-diffusion coefficient can be computed using the Einstein relation,[51]

$$D = \frac{1}{6t}\langle 2|\mathbf{r}(t) - \mathbf{r}(0)|^2\rangle \qquad (1)$$

that is valid only at sufficiently long time when the slope of a log−log plot of the mean square displacement (MSD) versus time shows a slope of unity. This usually requires a particle to escape from its solvation shell multiple times; that is, a MSD that reaches $(Mg_{max})^2$ where M is a suitable number of escapes and g_{max} is the location of the first peak in the like−like RDF.
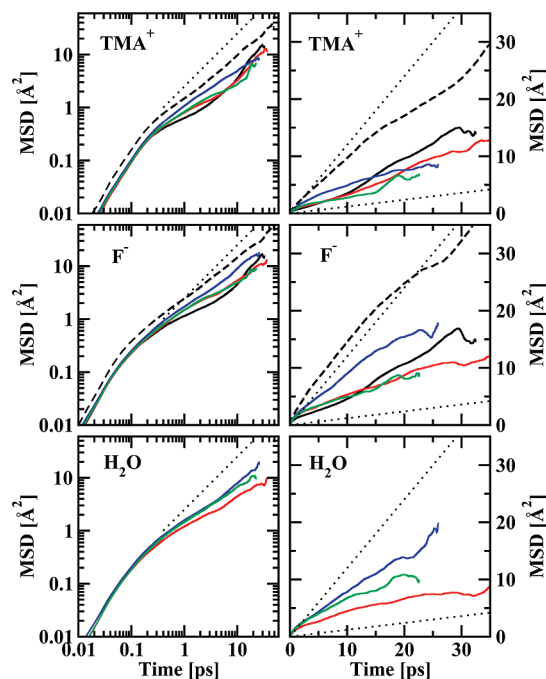
The MSD behavior during the production periods for anhydrous and hydrous TMAF is depicted in Figure 9. First, it is evident that the log−log plots of the MSDs for neither the ions nor the hydration water reach a slope of unity over the length of the current production periods. Second, given that $g_{max} > 6$ Å for the cations and anions, the simulations are only long enough to see these particles escape, on average, only once from their solvation shells. As one should expect, the simulation of the anhydrous form at 600 K shows somewhat larger MSDs for TMA^+ and F^- than the simulation for anhydrous TMAF at 400 K. Within the scatter of the MSD data, there appears to be no significant differences between the MSDs of the anhydrous and hydrous forms at 400 K nor between the MSDs of TMA^+, F^-, and H_2O, whereas longer simulations of ionic liquids using molecular mechanics force fields indicated enhanced transport and relaxation upon addition of water.[52] Cautiously, we estimate that the diffusion coefficients for all species in anhydrous and hydrous TMAF fall into the range from 0.2 to 2.0×10^{-5} cm^2 s^{-1}.

4. Conclusions

First principle molecular dynamics simulations in the isobaric−isothermal ensemble were carried out to investigate the liquid phase of pure tetramethyl ammonium fluoride (TMAF), its equimolar mixture with water, and its dilute solution in water. The simulations indicate that significant structural rearrangement and changes in cohesive energy density and compressibility occur upon addition of water. In agreement with experimental observations, anhydrous TMAF is found to decompose into trimethylamine and fluoromethane at elevated temperatures, whereas formation of hydrofluoric acid is not observed.

For the equimolar mixture, simulations were carried out using two different generalized gradient approximation functionals and

two values of the charge density cutoff, and it is found that thermodynamic properties are rather sensitive to these details of the electronic structure calculations, whereas structural characteristics are less sensitive to the choice of electronic structure parameters. In anhydrous TMAF, the ions are coordinated on average to four counterions, but the F−N coordination number decreases to about 3 for hydrous TMAF. The hydration water in hydrous TMAF mostly associates with either one or two fluoride ions, and lifetimes for these H-bonds often extend beyond 20 ps. Analysis of the MSDs shows no significant differences either between the anhydrous and hydrous forms or among the different species in these systems.

References and Notes

(1) Welton, T. *Chem. Rev.* **1999**, *99*, 2071.
(2) Wilkes, J. S. *Green Chem.* **2002**, *4*, 73.
(3) Rogers, R. D.; Seddon, K. R. *Science* **2003**, *302*, 792.
(4) Huddleston, J. G.; Rogers, R. D. *Chem. Commun.* **1998**, *16*, 1765.
(5) Sheldon, R. *Chem. Commun.* **2001**, *23*, 2399.
(6) Parvulescu, V.; Hardacre, C. *Chem. Rev.* **2007**, *107*, 2615.
(7) Seddon, K. R.; Stark, A.; Torres, M. J. *Pure Appl. Chem.* **2000**, *72*, 2275.
(8) Cammsrata, L.; Kazarian, S. G.; Salter, P. A.; Welton, T. *Phys. Chem. Chem. Phys.* **2001**, *3*, 5192.
(9) Swatloski, R. P.; Spear, S. K.; Holbrey, J. D.; Rogers, R. D. *J. Am. Chem. Soc.* **2002**, *124*, 4974.
(10) Swatloski, R. P.; Holbrey, J. D.; Rogers, R. D. *Green Chem.* **2003**, *5*, 361.
(11) Maiti, A.; Pagoria, P. F.; Gash, A. E.; Han, T. Y.; Orme, C. A.; Gee, R. H.; Fried, L. E. *Phys. Chem. Chem. Phys.* **2008**, *10*, 5050.
(12) Lawson, A.; Collie, N. *J. Chem. Soc.* **1888**, *53*, 624.
(13) Christe, K.; Wilson, W.; Wilson, R.; Bau, R.; Feng, J. *J. Am. Chem. Soc.* **1990**, *112*, 7619.
(14) Christe, K.; Jenkins, H. D. B. *J. Am. Chem. Soc.* **2003**, *125*, 9457.
(15) Menand, M.; Dalla, V. *Synlett* **2005**, 95.
(16) Staben, D.; Mootz, D. *Z. Naturforsch. B* **1993**, 1057.
(17) Lynden-Bell, R. M.; Del Popolo, M. G.; Youngs, T. G. A.; Kohanoff, J.; Hanke, C. G.; Harper, J. B.; Pinilla, C. C. *Acc. Chem. Res.* **2007**, *40*, 1138.
(18) Padua, A. A. H.; Gomes, M. F.; Lopes, J. N. A. C. *Acc. Chem. Res.* **2007**, *40*, 1087.
(19) Margulis, C.; Hu, Z. *Acc. Chem. Res.* **2007**, *40*, 1097.
(20) Maginn, E. *Acc. Chem. Res.* **2007**, *40*, 1200.
(21) Wang, Y.; Jiang, W.; Yan, T.; Voth, G. A. *Acc. Chem. Res.* **2007**, *40*, 1193.
(22) Kirchner, B. *Top. Curr. Chem.* **2009**, *290*, 213.
(23) Lynden-Bell, R.; Atamas, N. A.; Vasilyuk, A.; Hanke, C. G. *Mol. Phys.* **2002**, *100*, 3225–3229.
(24) Jiang, W.; Wang, Y.; Voth, A. *J. Phys. Chem. B* **2007**, *111*, 4812.
(25) Spickermann, C.; Thar, J.; Lehmann, S. B. C.; Zahn, S.; Hunger, J.; Buchner, R.; Hunt, P. A.; Welton, T.; Kirchner, B. *J. Chem. Phys.* **2008**, *129*, 104505.
(26) Hanke, C.; Lynden-Bell, R. *J. Phys. Chem. B* **2003**, *107*, 10873–10878.
(27) VandeVondele, J.; Krack, M.; Mohamed, F.; Parrinello, M.; Chassaing, T.; Hutter, J. *Comput. Phys. Commun.* **2005**, *167*, 103.
(28) Lippert, G.; Hutter, J.; Parrinello, M. *Mol. Phys.* **1997**, *92*, 477.
(29) Kohn, W.; Sham, L. J. *Phys. Rev. A* **1965**, *140*, A1133.
(30) Becke, A. D. *Phys. Rev. A* **1988**, *38*, 3098.
(31) Lee, C. T.; Yang, W. T.; Parr, R. G. *Phys. Rev. B* **1988**, *37*, 785.
(32) Goedecker, S.; Teter, M.; Hutter, J. *Phys. Rev. B* **1996**, *54*, 1703.
(33) Hartwigsen, C.; Goedecker, S.; Hutter, J. *Phys. Rev. B* **1998**, *58*, 3641.
(34) Perdew, J.; Burke, K.; Ernzerhof, M. *Phys. Rev. Lett.* **1996**, *77*, 865.
(35) Martyna, G. J.; Klein, M. L.; Tuckerman, M. E. *J. Chem. Phys.* **1992**, *97*, 2635.
(36) Jochen Schmidt, J.; VandeVondele, J.; Kuo, I.-F. W.; Sebastiani, D.; Siepmann, J. I.; Hutter, J.; Mundy, C. J. *J. Phys. Chem. B* **2009**, *113*, 11959.
(37) Wick, C. D.; Stubbs, J.; Rai, N.; Siepmann, J. *J. Phys. Chem. B* **2005**, *109*, 18974.
(38) Berendsen, H. J. C.; Grigera, J. R.; Straatsma, T. P. *J. Phys. Chem.* **1987**, *91*, 6269.
(39) McGrath, M. J.; Siepmann, J. I.; Kuo, I. W.; Mundy, C. J.; VandeVondele, J.; Hutter, J.; Mohamed, F.; Krack, M. *ChemPhysChem* **2005**, *6*, 1894.
(40) McGrath, M. J.; Siepmann, J. I.; Kuo, I. W.; Mundy, C. J. *Mol. Phys.* **2006**, *106*, 3619.
(41) McGrath, M. J.; Siepmann, J. I.; Kuo, I. W.; Mundy, C. J.; VandeVondele, J.; Hutter, J.; Mohamed, F.; Krack, M. *J. Phys. Chem. A* **2006**, *110*, 640.
(42) Shah, J.; Maginn, E. *Fluid Phase Equilib.* **2004**, *222*, 195.
(43) Kell, G. *J. Chem. Eng. Data* **1970**, *15*, 119.
(44) Martin, M. G.; Siepmann, J.; Schure, M. R. *J. Phys. Chem. B* **1999**, *103*, 11191.
(45) Roethlisberger, U.; Parrinello, M. *J. Chem. Phys.* **1997**, *106*, 4658.
(46) Stubbs, J.; Siepmann, J. *J. Am. Chem. Soc.* **2005**, *127*, 4722.
(47) Chen, B.; Siepmann, J. *J. Phys. Chem. B* **2006**, *110*, 3555.
(48) Kuo, I.-F.; Mundy, C.; Eggimann, B.; McGrath, M.; Siepmann, J.; Chen, B.; Vieceli, J.; Tobias, D. *J. Phys. Chem. B* **2006**, *110*, 3738.
(49) Hanke, C. G.; Atamas, N. A.; Lynden-Bell, R. *Green Chem.* **2002**, *4*, 107–111.
(50) Kuo, I.-F.; Mundy, C.; McGrath, M.; Siepmann, J. *J. Chem. Theor. Comput.* **2006**, *2*, 1274.
(51) Allen, M. P.; Tildesley, D. J. *Computer Simulation of Liquids*; Clarendon Press: Oxford: 1987.
(52) Annapureddy, H.; Hu, Z. H.; Xia, J.; Margulis, C. *J. Phys. Chem. B* **2008**, *112*, 1770.

JP104261H